Incorporating Microporous Zn_3 and Zn_2Cd MOFs into Pebax/PVDF Mixed Matrix Membranes for improved Carbon Dioxide Separation Performance.

Mahsan Basafa,[a] Amanda P. Parsons,[a] Ellan K. Berdichevsky,[a] Mason C. Lawrence, [a] Michael J. Katz,[a]*

[a]Department of Chemistry, Memorial University of Newfoundland, St. John's, Newfoundland and Labrador A1C 5S7, Canada

KEYWORDS: Gas separation, Mixed matrix membranes, Pebax® 30R51, PVDF Kynar® 761, Zn-based MOFs, molecular sieving, microporous materials.

ABSTRACT: A pair of related metal-organic framework (**Zn_3** and **Zn_2Cd**) developed in our group were incorporated into Pebax® 30R51 and PVDF Kynar® 761 polymers to fabricate mixed matrix membranes (MMMs). These MOFs were chosen due to the carbon dioxide molecular sieving ability of **Zn_3**, and the slightly larger pore aperture of **Zn_2Cd** that allows carbon dioxide and larger gases to enter the pores. For Pebax-based MMMs, this work demonstrated an over two-fold and four-and-a-half-fold increase in carbon dioxide permeability for **Zn_3**- (15 wt%) and **Zn_2Cd**-containing (10 wt%) MMMs over the pristine polymer. Separation selectivity (CO_2:N_2) of 4.21 and 7.33 were observed for **Zn_3** and **Zn_2Cd** (10 wt%). For PVDF-based MMMs, the incorporation of **Zn_3** and **Zn_2Cd** (10 wt%) increased the carbon dioxide permeability approximately two- and three-fold. The CO_2/N_2 selectivity of the PVDF membranes increased 73% (1.01 to 1.86) and 68% (1.01 to 1.68) when 15 wt% **Zn_3** and **Zn_2Cd** were incorporated into PVDF. The improved performance of Pebax over PVDF based MMMs is attributed to matching the permeability of the polymer bulk phase (Pebax over PVDF) and the dispersed phase (**Zn_3** and **Zn_2Cd)**. The lower permeability allows the MOF, which has slow kinetics associated with molecular sieving, to participate in the permeation process better. With regards to **Zn_3** vs. **Zn_2Cd**, while **Zn_3** acts as a molecular sieve and **Zn_2Cd** does not, we hypothesize that the faster diffusion of carbon dioxide gas in **Zn_2Cd** can out-compete the lower nitrogen gas permeability and molecular sieving properties of **Zn_3**. However, we expect that further increasing the pore aperture would increase the permeabilities of nitrogen gas such that differences in diffusion kinetics due to molecular size would be unimportant.

Introduction

In order to slow down and ideally reverse climate change, while improving air quality, it is crucial that greenhouse gas emissions (i.e., carbon dioxide, methane, nitrous oxide, and water vapour) are reduced.[1] Ideally, society would transition to a net-zero emission economy in which emission sources are phased out, or otherwise captured or utilized to form value-added products.[2-4] One of the leading anthropogenic greenhouse gases is carbon dioxide.[2] In this regard, carbon capture technologies (either direct air capture (DAC), or direct capture from emission sources such as flue gas) play an important role in society as we transition into a net-zero economy.[5-9]

Carbon capture can be accomplished by utilizing materials/systems that excel at separating carbon dioxide from a complex mixture, storing carbon dioxide, or simultaneously separating and storing carbon dioxide from a complex mixture.[5, 9-12] Materials that focus solely on separating carbon dioxide (i.e., kinetic-based separations) require that carbon dioxide – which has the smallest kinetic diameter between nitrogen, oxygen, and carbon dioxide – traverses a material faster than the other gases in a matrix.[13-15] Kinetic separations have several advantages. For DAC, the partial pressure of carbon dioxide is low (ca. 400 ppm). Adsorptive materials would require high adsorption enthalpies, and thus energetically demanding desorption, to operate at these partial pressures.[8] Conversely, kinetic separations can operate at low partial pressures as long as the kinetics of gas separation are faster for carbon dioxide; this would allow for pre-concentration prior to adsorption/utilization.[4-5] For exhaust emissions, kinetic separation improves with temperature and requires less material than adsorption; this is beneficial in offshore applications where space is at a premium.

Given the importance of carbon capture technology and the benefits of kinetic-based separations, the design of materials capable of kinetically separating carbon dioxide from a complex mixture is of great interest. With that in mind we have been working on porous materials, specifically metal-organic frameworks (MOFs), whose pore apertures are designed for kinetic separations.[13] MOFs consist of metal ions interconnected by organic linkers. With judicious choice of the node and linker(s), the size and shape of the pore and pore aperture as well as the functional group that decorate the pore can be tuned towards a specific application.[16-18] Coupled with their high thermal and mechan-

ical stability, MOFs have been used in variety of applications.[19-23]

For efficient kinetic separations, MOFs require pore apertures that are smaller than the kinetic diameter of nitrogen gas (3.64 Å) but larger than carbon dioxide (3.30 Å).[24] Under these conditions, the MOF behaves as a molecular sieve. We have recently reported a new family of MOFs (Figure 1) having the formula $Zn_2M(NH_2BDC)_3(DABCO)$ (M = Zn, Cd).[13] From the vantage point of a gas molecule entering the porous structure, this family of MOFs consists of a donut-shaped pore formed via a hexagonal outer edge and a DABCO-shaped inner edge core (Figure 1). The size of the pore aperture when M = Zn (**Zn_3**) has been computationally and experimentally measured to be between the kinetic diameter of carbon dioxide and nitrogen gas. This suggests that **Zn_3** is a molecular sieve for carbon dioxide. When the pore aperture was enlarged slightly (M = Cd, **Zn_2Cd**), we observed that both gases are able to enter the pores of the MOF. However, the kinetics for carbon dioxide gas transport are likely faster than for nitrogen gas transport. These new MOFs offer an opportunity to study molecular sieving and the importance of sub-angstrom changes in pore apertures of the size of the kinetic diameter of gases.

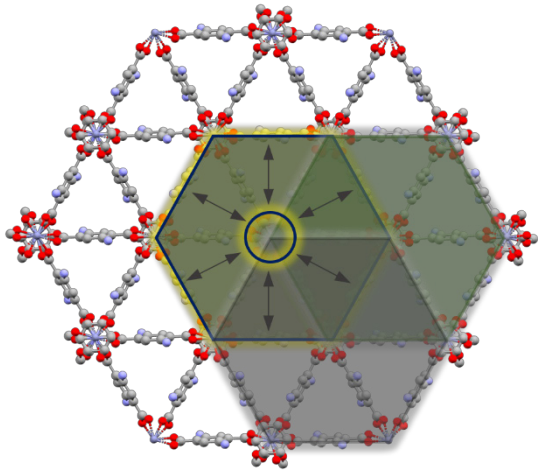

Figure 1: Crystal structure of **Zn_3** viewed down the *c*-axis. Each hexagon represents the shape of one pore. Through the centre of each hexagonal shaped pore passes a DABCO unit (circle). From a gas molecules perspective, the pores appear as hexagons with the center blocked. Thus, each pore aperture (3.3 Å; arrows) can be viewed as a donut shaped pore (4.8 Å wide) consisting of a hexagonal outer edge. Three hexagon layers (illustrated by the three hexagons in the figure) stack to form the triangular appearing structure. The network topology of **Zn_3** and **Zn_2Cd** is **bcu**. Hydrogens and solvent molecules are omitted for clarity.

As stated above, kinetic separations require less material because the material acts as a gate for carbon dioxide to travel through.[9, 12, 25-26] Given MOFs are crystalline powders, making a perfect gate requires the incorporation of MOFs into a matrix such as a polymeric membrane (i.e., mixed-matrix membranes; MMMs). Polymeric membranes are modular, easy to scale-up, and the low capital and operating costs, low energy requirements, and ease of operation are among the advantages of membrane separation processes[27]

The synthesis and applications of MOF-containing MMMs is an emerging area of MOF chemistry.[14, 25, 28-31] For example, an allyl-substituted derivative of the MOF UiO-66[29] was covalently grafted with polydimethylsiloxane (PDMS) to form a thin, flexible, defect-free MMM. It was demonstrated that the MMMs prepared from PDMS-coated MOF particles resulted in membranes with high carbon dioxide permeability (4573 ± 727 Barrer) without a loss in CO_2/N_2 selectivity (CO_2/N_2 selectivity of 10.0 ± 1.0) compared to PDMS-only membranes. Venna and co-workers examined MMMs of UiO-66-NH_2 in a Matrimid® glassy polymer.[29, 32] An increase in the carbon dioxide permeability (as much as 3 times) and CO_2/N_2 ideal selectivity (approximately, 1.2 times) was observed upon incorporation of 23 wt% UiO-66-NH_2.[32] At higher MOF loading (40 wt%), the ideal selectivity decreased. This was attributed to the formation of agglomerated clusters which act as non-selective diffusion pathways.

In the previous examples, UiO-66 and UiO-66-NH_2 have pore apertures that allow both nitrogen and carbon dioxide to enter the pores of the MOF. What remains to be explored is how MOFs that act as molecular sieves, where only one of the two gases can enter the pores, behave in MMM-based separations. To that end, with our ongoing interest in gas-phase applications of MOFs,[13, 33-34] the present work compares how molecular sieving in **Zn_3** and differences in diffusion kinetics in **Zn_2Cd** affect the separation properties of MMMs. The identical structure but small, sub-angstrom, changes in pore aperture offer a unique opportunity to explore the role of molecular sieving in separations. For this work we examined two different polymer hosts: polyether block amide copolymers (PEBA), commercialized under the tradename Pebax, and polyvinylidene fluoride (PVDF).

Pebax contains glassy rigid polyamide blocks separated by rubbery flexible polyether segments.[35-38] The former offers mechanical strength while the latter behaves as the permeable phase. Various polymeric membranes comprising both glassy and rubbery polymers are used for gas separation.[38-41] The separation performance of Pebax membranes is affected by the percentage and type of rigid and flexible segments in the block copolymer as well as the operating temperature.[38] The strong interactions between carbon dioxide and the polar linkages in the Pebax materials result in high carbon dioxide/nonpolar gas solubility selectivity in these polymers.[35, 38, 42-44]

PVDF is a hydrophobic polymer. Given that humidity is a concern under real-world conditions,[8] the use of a hydrophobic polymer may allow for improved separation efficiency and protection of the MOF from water adsorption. Furthermore, it is one of the most processable polymers due to low surface energy, good physical and mechanical properties, oxidation resistance, and thermal stability up to 140 °C.[45-47]

Experimental

Materials

Zinc nitrate hexahydrate ($Zn(NO_3)_2{\cdot}6H_2O$), cadmium nitrate tetrahydrate ($Cd(NO_3)_2{\cdot}4H_2O$), 2-aminoterephthalic acid (H_2-NH_2BDC), 4-diazabicyclo[2.2.2]octane (DABCO), dimethylsulfoxide (DMSO), methanol (MeOH), and

N,N-dimethylformamide (DMF) were purchased from commercial sources and were used without further purification. Pebax® 30R51, comprising 50 wt% polyamide (PA11) and 50 wt% polyethylene glycol (PEG) was donated from Arkema. Polyvinylidene fluoride (PVDF) was also provided from Arkema as a powder under the name Kynar® 761.

Characterizations

X-ray diffractograms were collected on a Rigaku miniflex equipped with a sealed-tube Cu target (λ = 1.54 Å) X-ray source operating at 40 kV and 15 mA and a D/teX Ultra detector.

Gas adsorption was measured on a Micromeritics 3Flex instrument. Prior to gas adsorption measurements, samples were degassed under vacuum for 18 hours while heating at 40 °C using Micromeritics Smart VacPrep instrument.

Scanning electron microscope (SEM) data was collected on FEI 650FEG at 5 kV or a JEOL JSM 7100F Field Emission SEM. Samples were gold coated using a SPI-Module Sputter Coater prior to analysis. For sample thicknesses, films were broken in half and mounted edge on to determine the cross-sectional thickness. Several different films were measured to get an average film thickness.

Gas separation performance measurement.

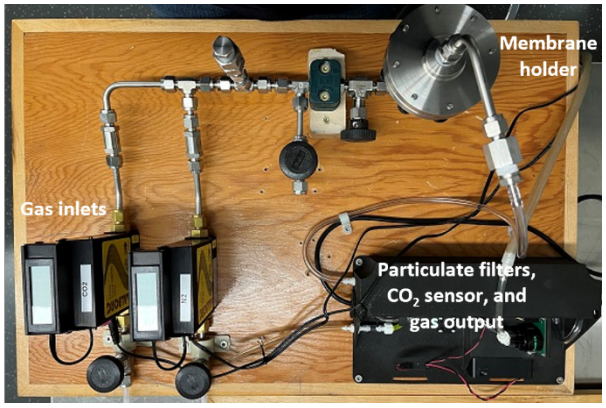

Figure 2: Schematic diagram of gas permeation test set up.

The pure carbon dioxide and nitrogen gas separation properties of MMMs was evaluated through an in-house custom-built gas separation apparatus using the constant pressure/variable volume method (Figure 2). The separation setup is equipped with mass flow meters, a membrane separation cell, particulate filters, a water trap, a carbon dioxide sensor, a pump, and an additional down-stream flow meter.

The effective surface area of tested membranes was 19.6 cm^2. All gas permeation tests were carried out at room temperatures (19-21 °C). The pure gas permeability (P_i) and the ideal selectivity (α_{ij}) of the membranes for a given gas pair are calculated by the solution-diffusion mechanism as follows:

$$P_i = \frac{Q_i l}{\Delta p_i A}, \alpha_{ij} = \frac{P_i}{P_j} \qquad (1)$$

P_i is the permeability coefficient of component *i* in Barrer (In SI units, 1 Barrer = 10^{-10} $cm^3STP \cdot cm \cdot cm^{-2} \cdot s^{-1} \cdot cmHg^{-1}$; in CGS units, 1 Barrer = 3.35×10^{-16} $mol \cdot m \cdot m^{-2} \cdot s \cdot Pa$). Permeability is defined as a measure of the flux of the gas through the material (volume of gas at STP/area of the film/unit time) multiplied by the thickness of the film and divided by the pressure difference across the film.

In the above equation, Q_i is the volume flow rate of component *i* on the permeate (post film) side ($cm^3 \cdot s^{-1}$, STP), *l* is the effective membrane thickness (cm), Δp_i is the pressure difference between the feed (pre film) and permeate side (cmHg), and *A* is the effective membrane area (cm^2).

The selectivity, α_{ij} of component *i* over *j* is the ratio of the permeability, and thus unit less. It is worth noting that while the permeability is subject to accurate film thickness and membrane area, the selectivity of a film requires only the volume flow rate and the pressure difference across the film.

Synthesis and characterization of ***Zn_3*** *and* ***Zn_2Cd***

Zn_3 and **Zn_2Cd** were synthesized and characterized according to the literature procedures.[13]

Fabrication and characterization of ***Zn_3*** *and* ***Zn_2Cd*** *mixed matrix membranes (MMMs).*

MMMs were prepared through solution casting method.[37] Prior to casting, **Zn_3** and **Zn_2Cd** were thermally degassed (activated) using a Micromeritics Smart VacPrep instrument. The samples were heated at 55 °C while a vacuum level below 1.00 mmHg was reached and then they were held under unrestricted vacuum for 18 hours.

Table 1: mass of Zn_3 and Zn_2Cd used to form MMMs with various loadings.

Polymer	Weight % in MMM	Mass of MOF used (mg)	
		Zn_3	Zn_2Cd
Pebax	5	7.4	7.4
	10	15.5	15.5
	15	24.7	24.7
	20	35	35
PVDF	5	5.3	5.3
	10	11.1	11.1
	20	25	25
	30	42.8	42.8

For Pebax-based MMMs, Pebax® 30R51 was selected due to the high solubility of Pebax® 30R51 in DMF at elevated temperatures; other available Pebax codes were less soluble or required solvent systems whose compatibility with Zn_3/Zn_2Cd have not been rigorously tested. To form the mixed matrix membrane, 140 mg of Pebax was dissolved in 4.8 mL of DMF (3 wt%) and heated in a sealed 4 Dram vial at 60 °C while stirring. Concurrently, **Zn_3** or **Zn_2Cd** was stirred for one hour in 1 mL of DMF (Table 1). To ensure good dispersion of the MOF in the MMM, we used the priming technique. In this method, approximately 10% of the polymer solution was added to the MOF suspension to "prime" the MOF particles. The solution was stirred for 4 hours at 60 °C and after homogenization, the remaining amount of polymer was added to the solution and stirred for an additional 4 hours at 60 °C. The obtained

solution was cast on a 7.6 cm wide, 2 mm deep Teflon mould. After solvent evaporation, at room temperature for 48 hours, the membrane delaminated from the mould. The membrane was stored at room temperature before further experimentation.

For PVDF-based MMMs, 100 mg of PVDF was dissolved in 953 µL of DMF (10 wt%) at room temperature while stirring. Concurrently, **Zn_3** or **Zn_2Cd** was stirred for one hour in 1 mL of DMF (Table 1). Using the priming technique, approximately 10% of the polymer solution was added to the MOF suspension. The solution was stirred for 4 hours at room temperature and after homogenization, the remaining amount of polymer was added to the solution and stirred for an additional 4 hours at room temperature. The obtained solution was cast on a 7.6 cm wide, 2 mm deep Teflon mould. After solvent evaporation at 70 °C overnight, the membrane delaminated from the mould. The membrane was stored at room temperature before further experimentation.

The thickness of the dried membranes varied from 40 to 65 µm. Increasing the MOF loading leads to an increase in the rigidity of the MMMs. At loadings in excess of 20 wt% MOF for Pebax-based MMMs and 40 wt% for PVDF-based MMMs, the membranes became too brittle to handle.

Results and Discussion

Synthesis and Characterization of MMMs

Zn_3 and **Zn_2Cd** were synthesized according to the literature procedures with gas adsorption properties and powder X-ray diffractograms consistent with those previously published.[13] MMMs of **Zn_3** and **Zn_2Cd** were made with either Pebax (5-20 wt% MOF) or PVDF (5-30 wt% MOF) as the polymer substrate. The films were made using a priming technique in which a small amount (10%) of polymer solution is allowed to mix with the MOF/solvent suspension prior to polymer/MOF incorporation and casting. The MMMs were cast in Teflon moulds where they readily delaminated upon drying.

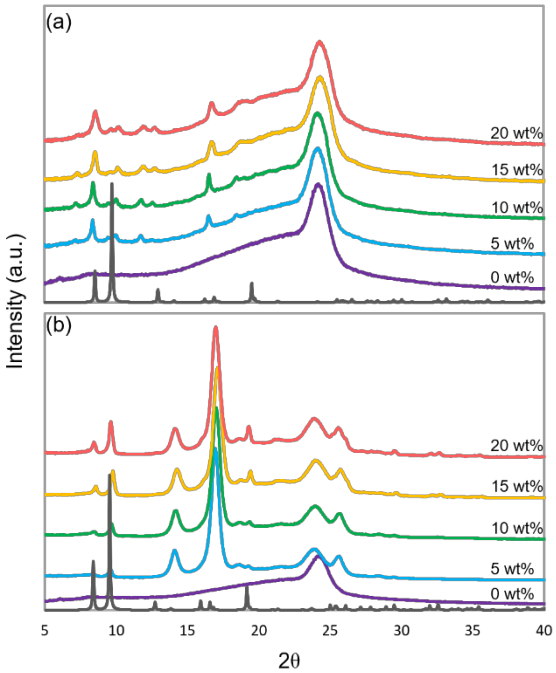

Figure 3: Powder X-ray diffractograms of Pebax-containing MMMs with (a) **Zn_3**, and (b) **Zn_2Cd**. Gray traces represent the simulated diffractogram of the MOF.

The powder X-ray diffractograms of Pebax and PVDF-based MMMs of **Zn_3** and **Zn_2Cd** are shown in Figure 3. Pristine Pebax films exhibit a broad peak between 10° and 20° in 2θ, characteristic of the amorphous rubbery polyether phase and a distinct peak at 23° in 2θ representing the crystalline glassy polyamide phase. In both the **Zn_3** and **Zn_2Cd** MMMs, the peaks associated with Pebax remain visible. This indicates that the crystallinity of the polymer matrix remains relatively unchanged upon MOF incorporation. Furthermore, the diffraction peaks associated with **Zn_3** and **Zn_2Cd** match well with the diffraction data simulated from the crystal structures of these MOFs. Some degree of preferred orientation is observed in the PXRD plots, as demonstrated by the higher-than-expected intensity for the peaks ca. 17 ° in 2θ; this is more pronounced in **Zn_2Cd** due to the higher scattering factor for Cd vs. Zn.

The powder X-ray diffractogram of PVDF (Figure 4) shows one strong Bragg diffraction peak at 18.2°; three weaker and slightly broader peaks at 20.5°, 27.0°, and 33.5° and one broad peak consistent with amorphous behaviour ranging from 14-30° in 2θ are also observed. As **Zn_3** and **Zn_2Cd** are incorporated in PVDF the crystalline diffraction peaks of the polymer disappear. The change in crystallinity for PVDF upon MOF incorporation indicates that the MOF is well-mixed with PVDF. The crystallinity of **Zn_3** and **Zn_2Cd** were consistent with the simulated diffractograms of these materials. **Zn_3**, especially at high (20 wt%) loadings, indicated the presence of an additional phase; for the purpose of this work, this does not appear to affect the results and conclusions.

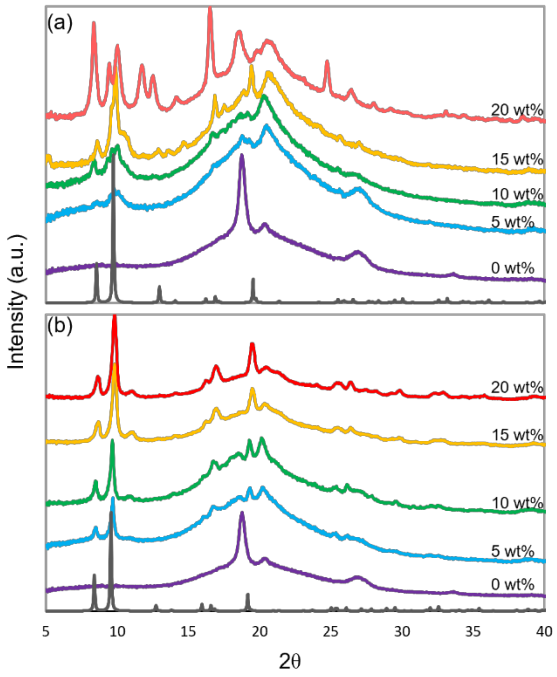

Figure 4: Powder X-ray diffractograms of PVDF-containing MMMs with (a) **Zn_3**, and (b) **Zn_2Cd**. Gray traces represent the simulated diffractogram of the MOF.

To further investigate the MMMs, the scanning electron micrographs (SEMs) of the surface were measured (Figure

5). Both pristine Pebax and PVDF show a smooth morphology (Figure 5a and d). Independent of the MOF loadings, we see the same morphology changes for the MMMs (see supporting information, SI, for additional micrographs; Figure S1-S18).

For Pebax, when either 20 wt% **Zn_3** (Figure 5b) or **Zn_2Cd** (Figure 5c) is incorporated, the morphology of the film does not change significantly. The MMMs appear to show a homogeneous structure, with some MOF particles observed on the surface of the film. This illustrates that the MOF was well incorporated into the Pebax matrix and that the external surface area of the film is approximately the same as the observed geometric surface area (45 cm^2).

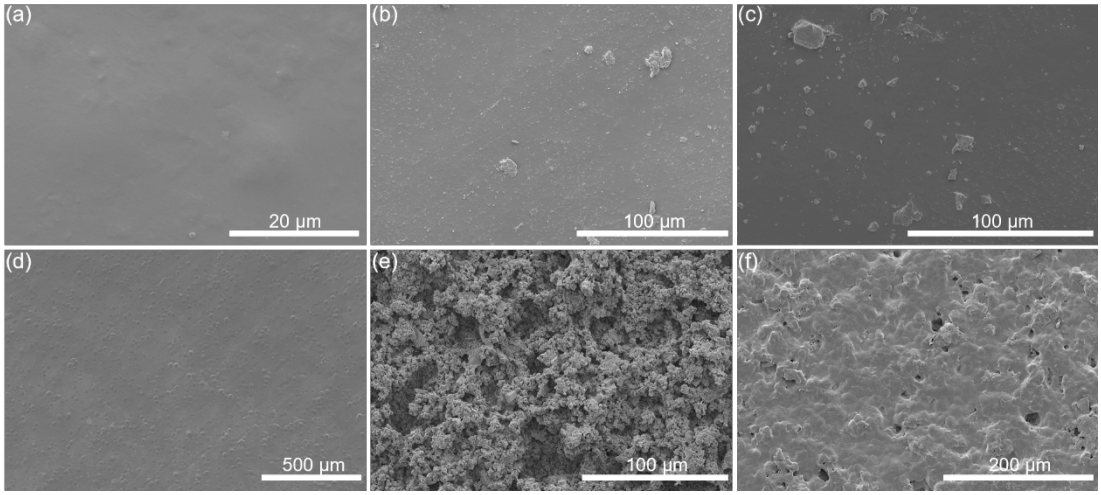

Figure 5: Scanning electron micrographs of (a) Pebax, (b) Pebax with 20 wt% **Zn_3**, (c) Pebax with 20 wt% **Zn_2Cd**, (d) PVDF, (e) PVDF with 30 wt% **Zn_3**, and (f) PVDF with 30 wt% **Zn_2Cd**.

For the PVDF-based MMMs we see a different behaviour. Upon inclusion of MOF (Figures 5d vs. e and f), the morphology of the MMM films changes significantly. The MMMs contain surface pores and an increased surface roughness. These surface pores, and thus the apparent external surface area, increases with MOF loading (See Figures S10 and S18 in the SI). Similar results have been observed in other studies.[48] This data is consistent with the powder X-ray diffractograms of the PVDF-based MMMs, which showed a decrease in crystallinity of the PVDF as the MOF is incorporated.

Gas Separation Performance of MMMs

The gas separation performance of the **Zn_3**- and **Zn_2Cd**-containing MMMs was measured on a custom-built instrumentation (Figure 2) equipped with upstream and downstream flow meters to measure flow rate and pressure drops across the membrane. The system operated in a conventional (i.e., dead-end/perpendicular) mode in which gas is forced through the MMM rather than a crossflow separation in which feed stream flows tangentially across the surface of the membrane. Relative to existing data on Pebax, our permeability values are higher.[49] We attribute this to the custom-built setup. However, the relative changes are meaningful and reflect the role of the MOF in the MMM.

Figure 6 illustrates the permeability and ideal selectivity (i.e., ratio of pure gas permeabilities) of Pebax-containing MMMs with **Zn_3** (Figure 6a) or **Zn_2Cd** (Figure 6b) as a function of MOF loading. The error in the permeability data was estimated to be between 8% and 10%. For the pristine Pebax film, the permeability to carbon dioxide gas is 1024 ± 100 Barrer and the permeability to nitrogen gas is 544 ± 50 Barrer (Table S1 in the SI). This results in a selectivity of 1.88 carbon dioxide to nitrogen gas molecules. For both **Zn_3**/Pebax MMMs and **Zn_2Cd**/Pebax MMMs, the lack of any major loss in selectivity compared to the pristine Pebax is observed, confirming the absence of large MOF-polymer interfacial defects.[19, 29, 42, 44, 50]

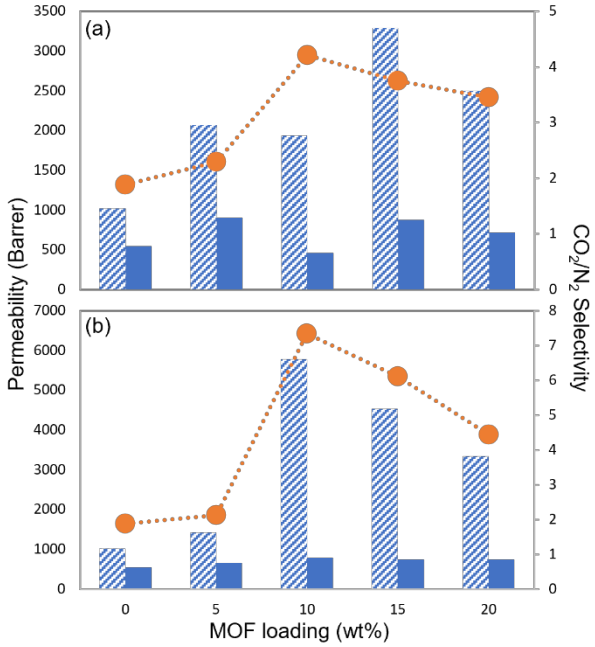

Figure 6: Permeability (CO_2: blue/white alternating; N_2: blue) and CO_2/N_2 selectivity (orange) of Pebax-based MMMs containing (a) **Zn_3** and (b) **Zn_2Cd** (see Table S1 of the SI for raw data).

As **Zn_3** is incorporated into Pebax, the carbon dioxide permeability increases more than that of nitrogen gas. This

leads to an increased selectivity. At 10 wt%, there is a maximum in the selectivity (4.21 CO_2/N_2). Interestingly, this increase seems to be due to a decrease in nitrogen gas permeability more than an increase in carbon dioxide permeability. Given the nominally flat films (Figure 5a-c), these results are reflective of the film properties and not changes in film morphology. Figure 6a illustrates that at these optimal loadings, nitrogen gas struggles to find a pathway through the MMM while carbon dioxide can utilize the MOF, albeit at slower kinetics than at lower MOF loadings, to pass through the MMM. The enhanced physical selectivity is thus based on the solution-diffusion mechanism which is improved upon incorporation of molecular sieve MOFs.[42, 44] At higher MOF loadings (15 and 20 wt%), however, the selectivity begins to decrease slightly (4.21 – 3.45 CO_2/N_2). Interestingly, the carbon dioxide gas permeability still increases from 10 to 15 wt%, but the nitrogen gas permeability beings to increase faster. This suggests that interparticle pathways are more operable at higher loadings. At 20 wt% **Zn_3**, the permeability begins to decrease for both nitrogen and carbon dioxide suggesting that the MOF is slowing down transport kinetics. Despite this, the selectivity of the MMMs remains above that of the pristine Pebax film, illustrating that the enhancement in the selectivity still dominates at these loadings. Higher MOF loadings produced films that were too brittle to work with.

Turning our attention to **Zn_2Cd**/Pebax MMMs, we once again see a change in selectivity and carbon dioxide permeability at 10 wt% (Figure 6b, Table S2 in the SI). The carbon dioxide permeability change between pristine Pebax and 10 wt% **Zn_2Cd** loaded Pebax is nearly 6 times larger with nearly no change in the nitrogen permeability. This can be attributed to the enhanced solubility and diffusivity towards carbon dioxide after **Zn_2Cd** is incorporated. As with **Zn_3**, higher **Zn_2Cd** loadings began to decrease the selectivity; this appears to be due to a decrease in carbon dioxide permeability rather than changes in nitrogen gas permeability (Table S1 in the SI).

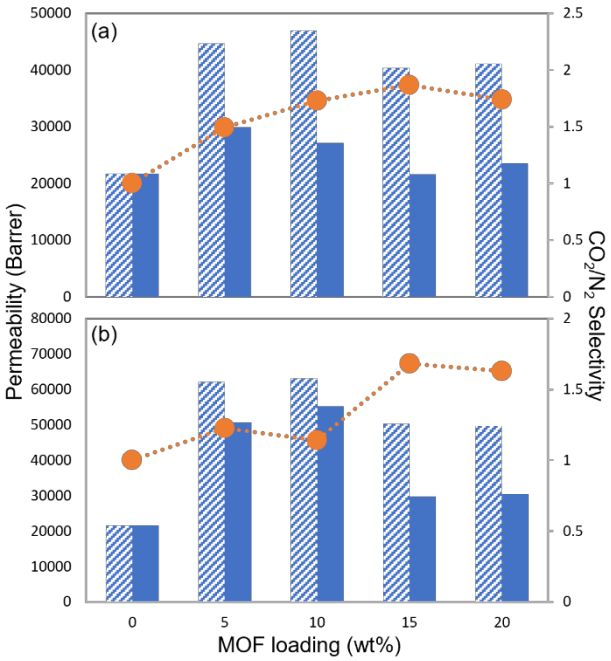

Figure 7: Permeability (CO_2: blue/white alternating; N_2: blue) and CO_2/N_2 selectivity (orange) of PVDF-based MMMs containing (a) **Zn_3** and (b) **Zn_2Cd**.

Turning our attention to PVDF-based MMMs (Figure 7), we note that the pristine PVDF film has a permeability of 21575 ± 2000 Barrer and 21682 ± 2000 Barrer for nitrogen and carbon dioxide gas, leading to a selectivity of approximately 1. These permeabilities are 20-fold higher than what was observed in pristine Pebax.

Incorporating **Zn_3** into PVDF resulted in a 2-fold or greater increased carbon dioxide permeability with at most a 50% increase in the nitrogen gas permeability. This led to a maximum selectivity of 1.86 CO_2/N_2. Incorporating **Zn_2Cd** into PVDF resulted in a 3-fold increase in permeability with a selectivity of 1.68.

Comparing the results between Pebax-based MMMs and PVDF-based MMMs, we conclude that polymers that have lower permeabilities (e.g., Pebax) can be more readily enhanced by incorporating a molecular sieving MOF, than polymers that have high permeabilities (PVDF). With carbon dioxide being only slightly smaller than the pore aperture of **Zn_3**, the permeation kinetics are necessarily slow. Thus, if the permeation kinetics of the polymer are not matched to the MOF, then interparticle diffusion pathways dominate and the MOF is not being utilized efficiently by the gas. This explains why gas separation performance of Pebax-based MMMs are enhanced by **Zn_3** and **Zn_2Cd** while PVDF-based MMMs show only a moderate enhancement.

Comparing **Zn_3** to **Zn_2Cd** MMMs with Pebax, we note that there are two different mechanisms in effect. Under optimal loading conditions (10 wt%), **Zn_3** is able to slow down nitrogen gas diffusion due to the inability of nitrogen gas to enter the porous structure. This forces nitrogen gas to utilize longer/slower interparticle pathways vs the direct path through the MOF used by carbon dioxide gas. For **Zn_2Cd**-containing Pebax MMMs we see an enhancement of carbon dioxide permeability without considerable change to the nitrogen gas permeability; this ultimately leads to the highest calculated separation selectivity. We hypothesize that the diffusion rate of carbon dioxide into **Zn_2Cd** is considerably faster than nitrogen gas. This is due to the 0.3 Å narrower kinetic diameter of carbon dioxide over nitrogen gas and a pore aperture that is slightly larger (estimated 4 Å) than nitrogen gas. Thus, for **Zn_2Cd**, both gas molecules can utilize the MOF, but carbon dioxide gas has faster kinetics and enhanced permeability selectivity.

For PVDF-based MMMs, comparing **Zn_3** to **Zn_2Cd** is far more challenging. It has been mentioned that obtaining favorable gas separation performance for pristine PVDF membranes has been a challenge. This is due to the large intersegmental distance in PVDF, which makes PVDF a suitable material for membrane support and using additives such as MOFs can enhance the PVDF membrane separation performance.[51] However, while carbon dioxide permeability is enhanced when the molecular sieving MOFs are incorporated, it is more likely that the morphology changes of the films (Figure 5) are the dominant factor in the observed performance metrics. The increase in the MOF loading increases porosity, and surface area vs. geometric surface area (Figure 5) of PVDF-based MMMs; Pebax-based MMMs appear to have near-identical surface

features in comparison. For PVDF, this results in an increase in the membrane flux. This suggests that for PVDF this is the dominant factor in improving the permeability changes with the MOF offering only modest enhancement from pore-based diffusion.

To ascertain if PVDF and Pebax block the pore apertures from carbon dioxide adsorption, we turned our attention to static carbon dioxide gas adsorption properties of the 10 wt% MMMs presented in this work (Figure S19-S20). For Pebax, the MOF incorporated MMMs show an increase in the gas adsorption properties. **Zn_2Cd** shows a marked improvement over the pristine Pebax film while **Zn_3** is only marginally better. This is expected given the ca. 2-fold increase in adsorption capacity of **Zn_2Cd** vs. **Zn_3**.[13] For PVDF-based MMMs, the two MOFs are able to increase the adsorption capacity, but there is little difference in the adsorption capacity between the MOFs. This suggests that the porosity of the PVDF may have increased (Figure 5) more than the MOF pores have enhanced the adsorption properties.

Conclusion

We examined the permeability and selectivity of two microporous MOFs that have very similar pore apertures whose sizes are approximately that of the kinetic diameter of nitrogen and carbon dioxide gas. From this work, we have demonstrated that matching the polymer-MOF properties to ensure the porous structure of the MOF is utilized is key to the successful utilization of microporous MOFs such as **Zn_3** and **Zn_2Cd**. Furthermore, we demonstrate a change of mode of action between **Zn_3** and **Zn_2Cd**. When a molecular sieve is used that has a pore aperture between the width of two gases, then enhancement seems to relate to the slowing down of the wider gas rather than the improvement of the narrower gas. However, when the molecular sieve has an aperture slightly larger than the two gases being explored, then we see enhancement due to improved kinetics of the thinner of the two gases. Looking forward, examining these polymers and other polymers under mixed gas conditions such as nitrogen/oxygen/carbon dioxide/water, and under direct-air-capture applications, will allow us to determine selectivity under more complex and real-life scenarios.

ASSOCIATED CONTENT

Supporting Information. Large format scanning electron micrographs and the gas transport and adsorption properties of the membranes are available free of charge via the Internet at http://pubs.acs.org.

AUTHOR INFORMATION

Corresponding Author

*Michael J. Katz – Department of Chemistry, Memorial University of Newfoundland, St. John's, Newfoundland and Labrador A1C 5S7, Canada; Email: mkatz@mun.ca

Author Contributions

The manuscript was written through contributions of all authors. All authors have given approval to the final version of the manuscript.

Funding Sources

The research was funded via the Natural Resources Canada (NRCan) Emission Reduction Fund. The funding was administered via Energy Research & Innovation Newfoundland (ERINL).

ACKNOWLEDGMENT

MJK acknowledges the Natural Resources Canada (NRCan) Emission Reduction Fund. The funding was administered via Energy Research & Innovation Newfoundland (ERINL). Additional funding was provided through NSERC (DG, RTI) and Department of Industry, Energy and Technology of Newfoundland (formally the Research & Development Corporation). We thank the Core Research Equipment & Instrument Training Network (CREAIT) at Memorial University for the use of their SEM facilities within the Micro Analysis Facility and The Earth Resources Research and Analysis (TERRA) Facility.

ABBREVIATIONS

A - Effective membrane area in cm^2

L - Effective membrane thickness in cm

P_i - Permeability coefficient of component i in Barrer (1 Barrer = 10^{-10} $cm^3STP \cdot cm \cdot cm^{-2} \cdot s^{-1} \cdot cmHg^{-1}$)

Q_i - Volume flow rate of component i on the permeate side ($cm^3 \cdot s^{-1}$, STP)

H_2-NH_2BDC - 2-aminoterephthalic acid

DABCO - 4-diazabicyclo[2.2.2]octane

DMF - *N,N*-dimethylformamide

DMSO - Dimethylsulfoxide

MeOH - Methanol

MMM - Mixed Matrix Membrane

MOF - Metal Organic Framework

PDMS - Polydimethylsiloxane

Pebax - Polyether block amide

PVDF - Polyvinylidene fluoride

PXRD - Powder X-ray diffractogram

SEM - Scanning electron microscope

Δp_i - Pressure difference between the feed and permeate side (cmHg)

TOC graphic:

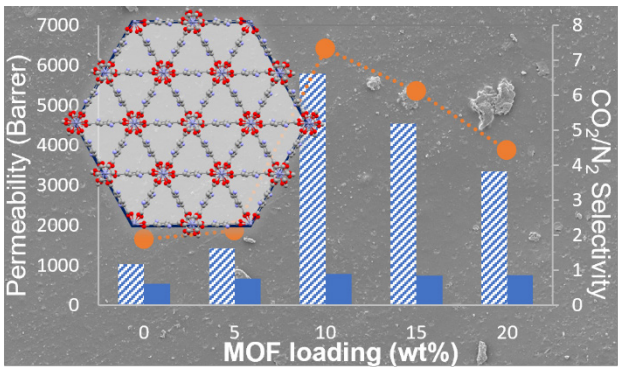

REFERENCES

1. Osman, A. I.; Hefny, M.; Abdel Maksoud, M. I. A.; Elgarahy, A. M.; Rooney, D. W., Recent advances in carbon capture storage and utilisation technologies: a review. *Environ. Chem. Lett.* **2021,** *19* (2), 797-849.

2. Fankhauser, S.; Smith, S. M.; Allen, M.; Axelsson, K.; Hale, T.; Hepburn, C.; Kendall, J. M.; Khosla, R.; Lezaun, J.; Mitchell-Larson, E.; Obersteiner, M.; Rajamani, L.; Rickaby, R.; Seddon, N.; Wetzer, T., The meaning of net zero and how to get it right. *Nat. Clim. Change* **2022,** *12* (1), 15-21.

3. DeAngelo, J.; Azevedo, I.; Bistline, J.; Clarke, L.; Luderer, G.; Byers, E.; Davis, S. J., Energy systems in scenarios at net-zero CO_2 emissions. *Nat. Commun.* **2021,** *12* (1), 6096.

4. *Carbon Dioxide Utilization to Sustainable Energy and Fuels*. 1st ed.; Springer Cham: 2022; p 353.

5. Siegelman, R. L.; Kim, E. J.; Long, J. R., Porous materials for carbon dioxide separations. *Nat. Mater.* **2021,** *20* (8), 1060-1072.

6. Erans, M.; Sanz-Pérez, E. S.; Hanak, D. P.; Clulow, Z.; Reiner, D. M.; Mutch, G. A., Direct air capture: process technology, techno-economic and socio-political challenges. *Energy Environ. Sci.* **2022,** *15* (4), 1360-1405.

7. Castro-Muñoz, R.; Zamidi Ahmad, M.; Malankowska, M.; Coronas, J., A new relevant membrane application: CO_2 direct air capture (DAC). *Chem. Eng. J.* **2022,** *446*, 137047.

8. Dods, M. N.; Weston, S. C.; Long, J. R., Prospects for Simultaneously Capturing Carbon Dioxide and Harvesting Water from Air. *Adv. Mater.* **2022,** *34* (38), 2204277.

9. Demir, H.; Aksu, G. O.; Gulbalkan, H. C.; Keskin, S., MOF Membranes for CO_2 Capture: Past, Present and Future. *Carbon Capture Sci. Technol.* **2022,** *2*, 100026.

10. Raganati, F.; Miccio, F.; Ammendola, P., Adsorption of Carbon Dioxide for Post-combustion Capture: A Review. *Energy Fuels* **2021,** *35* (16), 12845-12868.

11. Sharma, H.; Dhir, A., Capture of carbon dioxide using solid carbonaceous and non-carbonaceous adsorbents: a review. *Environ. Chem. Lett.* **2021,** *19* (2), 851-873.

12. Li, S.; Liu, Y.; Wong, D. A.; Yang, J., Recent Advances in Polymer-Inorganic Mixed Matrix Membranes for CO_2 Separation. *Polymers* **2021,** *13* (15), 2539.

13. Berdichevsky, E. K.; Downing, V. A.; Hooper, R. W.; Butt, N. W.; McGrath, D. T.; Donnelly, L. J.; Michaelis, V. K.; Katz, M. J., Ultrahigh Size Exclusion Selectivity for Carbon Dioxide from Nitrogen/Methane in an Ultramicroporous Metal–Organic Framework. *Inorg. Chem.* **2022,** *61* (20), 7970-7979.

14. Gong, H.; Nguyen, T. H.; Wang, R.; Bae, T.-H., Separations of binary mixtures of CO_2/CH_4 and CO_2/N_2 with mixed-matrix membranes containing $Zn(pyrz)_2(SiF_6)$ metal-organic framework. *J. Membr. Sci.* **2015,** *495*, 169-175.

15. Tu, R.; Zhang, W.; Zhang, J.; Wang, M.; Zhang, F.; Yang, K.; Li, J.; Pan, H.; Bernards, M. T.; Xie, P.; He, Y.; Shi, Y., Squarate-Calcium Metal–Organic Framework for Molecular Sieving of CO_2 from Flue Gas with High Water Vapor Resistance. *Energy Fuels* **2021,** *35* (17), 13900-13907.

16. Shekhah, O.; Liu, J.; Fischer, R. A.; Wöll, C., MOF thin films: existing and future applications. *Chem. Soc. Rev.* **2011,** *40* (2), 1081-1106.

17. Wang, Q.; Astruc, D., State of the Art and Prospects in Metal–Organic Framework (MOF)-Based and MOF-Derived Nanocatalysis. *Chem. Rev.* **2020,** *120* (2), 1438-1511.

18. Stavila, V.; Talin, A. A.; Allendorf, M. D., MOF-based electronic and opto-electronic devices. *Chem. Soc. Rev.* **2014,** *43* (16), 5994-6010.

19. Kanehashi, S.; Chen, G. Q.; Scholes, C. A.; Ozcelik, B.; Hua, C.; Ciddor, L.; Southon, P. D.; D'Alessandro, D. M.; Kentish, S. E., Enhancing gas permeability in mixed matrix membranes through tuning the nanoparticle properties. *J. Membr. Sci.* **2015,** *482*, 49-55.

20. Hao, L.; Libo, L.; Rui-Biao, L.; Wei, Z.; Zhangjing, Z.; Shengchang, X.; Banglin, C., Porous Metal-Organic Frameworks for Gas Storage and Separation: Status and Challenges. *EnergyChem* **2019,** *1* (1), 100006.

21. Ding, M.; Cai, X.; Jiang, H.-L., Improving MOF stability: approaches and applications. *Chem. Sci.* **2019,** *10* (44), 10209-10230.

22. Winarta, J.; Shan, B.; McIntyre, S. M.; Ye, L.; Wang, C.; Liu, J.; Mu, B., A Decade of UiO-66 Research: A Historic Review of Dynamic Structure, Synthesis Mechanisms, and Characterization Techniques of an Archetypal Metal–Organic Framework. *Cryst. Growth Des.* **2020,** *20* (2), 1347-1362.

23. Qazvini, O. T.; Babarao, R.; Telfer, S. G., Selective capture of carbon dioxide from hydrocarbons using a metal-organic framework. *Nat. Commun.* **2021,** *12* (1), 197.

24. Adil, K.; Belmabkhout, Y.; Pillai, R. S.; Cadiau, A.; Bhatt, P. M.; Assen, A. H.; Maurin, G.; Eddaoudi, M., Gas/vapour separation using ultra-microporous metal–organic frameworks: insights into the structure/separation relationship. *Chem. Soc. Rev.* **2017,** *46* (11), 3402-3430.

25. Kalaj, M.; Bentz, K. C.; Ayala, S., Jr.; Palomba, J. M.; Barcus, K. S.; Katayama, Y.; Cohen, S. M., MOF-Polymer Hybrid Materials: From Simple Composites to Tailored Architectures. *Chem. Rev.* **2020,** *120* (16), 8267-8302.

26. Kanehashi, S.; Scholes, C. A., Perspective of mixed matrix membranes for carbon capture. *Front. Chem. Sci. Eng.* **2020,** *14* (3), 460-469.

27. Wang, X.; Song, C., Carbon Capture From Flue Gas and the Atmosphere: A Perspective. *Front. Energy Res.* **2020,** *8*, 560849.

28. Liu, F.; Wang, T.; Dong, H.; Liu, W., Modified metal–organic framework by a novel coordinatively unsaturated amine grafting mechanism for direct air capture of CO_2. *Chem. Eng. J.* **2023,** *454*, 140431.

29. Katayama, Y.; Bentz, K. C.; Cohen, S. M., Defect-Free MOF-Based Mixed-Matrix Membranes Obtained by Corona Cross-Linking. *ACS Appl. Mater. Interfaces* **2019,** *11* (13), 13029-13037.

30. Martínez-Izquierdo, L.; Téllez, C.; Coronas, J., Highly stable Pebax® Renew® thin-film nanocomposite membranes with metal organic framework ZIF-94 and ionic liquid $[Bmim][BF_4]$ for CO_2 capture. *J. Mater. Chem. A* **2022,** *10* (36), 18822-18833.

31. Ge, B.; Xu, Y.; Zhao, H.; Sun, H.; Guo, Y.; Wang, W., High Performance Gas Separation Mixed Matrix Membrane Fabricated by Incorporation of Functionalized Submicrometer-Sized Metal-Organic Framework. *Materials* **2018,** *11* (8), 1421.

32. Venna, S. R.; Lartey, M.; Li, T.; Spore, A.; Kumar, S.; Nulwala, H. B.; Luebke, D. R.; Rosi, N. L.; Albenze, E., Fabrication of MMMs with improved gas separation properties using externally-functionalized MOF particles. *J. Mater. Chem. A* **2015,** *3* (9), 5014-5022.

33. McGrath, D. T.; Ryan, M. D.; MacInnis, J. J.; VandenBoer, T. C.; Young, C. J.; Katz, M. J., Selective decontamination of the reactive air pollutant nitrous acid via node-linker cooperativity in a metal–organic framework. *Chem. Sci.* **2019,** *10* (21), 5576-5581.

34. Lawrence, M. C.; Katz, M. J., Analysis of the Water Adsorption Isotherms in UiO-Based Metal–Organic Frameworks. *J. Phys. Chem. C* **2022,** *126* (2), 1107-1114.

35. Bondar, V. I.; Freeman, B. D.; Pinnau, I., Gas sorption and characterization of poly(ether-b-amide) segmented block copolymers. *J. Polym. Sci., Part B: Polym. Phys.* **1999,** *37* (17), 2463-2475.

36. Car, A.; Stropnik, C.; Yave, W.; Peinemann, K.-V., Pebax®/polyethylene glycol blend thin film composite membranes for CO_2 separation: Performance with mixed gases. *Sep. Purif. Technol.* **2008,** *62* (1), 110-117.

37. Embaye, A. S.; Martínez-Izquierdo, L.; Malankowska, M.; Téllez, C.; Coronas, J., Poly(ether-block-amide) Copolymer Membranes in CO_2 Separation Applications. *Energy Fuels* **2021,** *35* (21), 17085-17102.

38. Martínez-Izquierdo, L.; Perea-Cachero, A.; Malankowska, M.; Téllez, C.; Coronas, J., A comparative study between single gas and mixed gas permeation of polyether-block-amide type copolymer membranes. *J. Environ. Chem. Eng.* **2022,** *10* (5), 108324.

39. Powell, C. E.; Qiao, G. G., Polymeric CO_2/N_2 gas separation membranes for the capture of carbon dioxide from power plant flue gases. *J. Membr. Sci.* **2006,** *279* (1), 1-49.

40. Xie, K.; Fu, Q.; Qiao, G. G.; Webley, P. A., Recent progress on fabrication methods of polymeric thin film gas separation membranes for CO_2 capture. *J. Membr. Sci.* **2019,** *572*, 38-60.

41. Han, Y.; Yang, Y.; Ho, W. S. W., Recent Progress in the Engineering of Polymeric Membranes for CO_2 Capture from Flue Gas. *Membranes* **2020,** *10* (11), 365.

42. Sutrisna, P. D.; Hou, J.; Li, H.; Zhang, Y.; Chen, V., Improved operational stability of Pebax-based gas separation membranes with ZIF-8: A comparative study of flat sheet and composite hollow fibre membranes. *J. Membr. Sci.* **2017,** *524*, 266-279.

43. Khosravi, T.; Omidkhah, M.; Kaliaguine, S.; Rodrigue, D., Amine-functionalized CuBTC/poly(ether-b-amide-6) (Pebax® MH 1657) mixed matrix membranes for CO_2/CH_4 separation. *Can. J. Chem. Eng.* **2017,** *95* (10), 2024-2033.
44. Zhang, N.; Wu, H.; Li, F.; Dong, S.; Yang, L.; Ren, Y.; Wu, Y.; Wu, X.; Jiang, Z.; Cao, X., Heterostructured filler in mixed matrix membranes to coordinate physical and chemical selectivities for enhanced CO_2 separation. *J. Membr. Sci.* **2018,** *567*, 272-280.
45. Ahmadi Feijani, E.; Tavasoli, A.; Mahdavi, H., Improving Gas Separation Performance of Poly(vinylidene fluoride) Based Mixed Matrix Membranes Containing Metal–Organic Frameworks by Chemical Modification. *Ind. Eng. Chem. Res.* **2015,** *54* (48), 12124-12134.
46. Ahmad, N. A.; Mohd Noh, A. N.; Leo, C. P.; Ahmad, A. L., CO_2 removal using membrane gas absorption with PVDF membrane incorporated with POSS and SAPO-34 zeolite. *Chem. Eng. Res. Des.* **2017,** *118*, 238-247.
47. Pagliero, M.; Comite, A.; Soda, O.; Costa, C., Effect of support on PVDF membranes for distillation process. *J. Membr. Sci.* **2021,** *635*, 119528.
48. Yuan, X.-T.; Xu, C.-X.; Geng, H.-Z.; Ji, Q.; Wang, L.; He, B.; Jiang, Y.; Kong, J.; Li, J., Multifunctional PVDF/CNT/GO mixed matrix membranes for ultrafiltration and fouling detection. *J. Hazard. Mater.* **2020,** *384*, 120978.
49. Li, M.; Zhang, X.; Zeng, S.; bai, L.; Gao, H.; Deng, J.; Yang, Q.; Zhang, S., Pebax-based composite membranes with high gas transport properties enhanced by ionic liquids for CO_2 separation. *RSC Advances* **2017,** *7* (11), 6422-6431.
50. Ahmad, M. Z.; Navarro, M.; Lhotka, M.; Zornoza, B.; Téllez, C.; de Vos, W. M.; Benes, N. E.; Konnertz, N. M.; Visser, T.; Semino, R.; Maurin, G.; Fila, V.; Coronas, J., Enhanced gas separation performance of 6FDA-DAM based mixed matrix membranes by incorporating MOF UiO-66 and its derivatives. *J. Membr. Sci.* **2018,** *558*, 64-77.
51. Ashtiani, S.; Khoshnamvand, M.; Číhal, P.; Dendisová, M.; Randová, A.; Bouša, D.; Shaliutina-Kolešová, A.; Sofer, Z.; Friess, K., Fabrication of a PVDF membrane with tailored morphology and properties via exploring and computing its ternary phase diagram for wastewater treatment and gas separation applications. *RSC Advances* **2020,** *10* (66), 40373-40383.